Appl. Magn. Reson. 21, 549–561 (2001)

Applied
Magnetic Resonance

Single-Crystal EPR Studies of Transition-Metal Ions in Inorganic Crystals at Very High Frequency

S. K. Misra[1], S. I. Andronenko[1], K. A. Earle[2], and J. H. Freed[2]

[1] Physics Department, Concordia University, Montreal, Quebec, Canada
[2] Baker Laboratory, Department of Chemistry and Chemical Biology, Cornell University, Ithaca, New York, USA

Received October 10, 2001

Abstract. Electron paramagnetic resonance (EPR) single-crystal rotation studies at very high frequency (249.9 GHz) of transition metal ions with electron spins greater than one-half are reported. At 249.9 GHz, the spectra are in the high-field limit despite large zero-field splittings. This leads to a considerable simplification of the spectra, and aids in their interpretation. Single-crystal 249.9 GHz EPR spectra of Ni^{2+} in $Ni_2CdCl_6 \cdot 12H_2O$, Mn^{2+} (0.2%) in ZnV_2O_7, and Fe^{3+} (2%) in $CaYAlO_4$ were recorded at 253 K in an external magnetic field of up to 9.2 T, along with those at X-band and Q-band frequencies at 295 K and lower temperatures. The goniometer used at 249.9 GHz for single-crystal rotation is based on a quasi-optical design and is an integral part of a special Fabry-Pérot resonator. The values of the spin-Hamiltonian parameters were estimated from a simultaneous fitting of all of the observed line positions at several microwave frequencies recorded at various orientations of each crystal with respect to the external magnetic field with least-squares fitting in conjunction with matrix diagonalization. Estimates of zero-field splitting parameter D at room temperature are: for Ni^{2+}, about −31 GHz (site I) and about −7 GHz (site II); for Mn^{2+}, about 6 GHz; and for Fe^{3+}, about 29 GHz.

1 Introduction

Recently, advances in magnet and millimeter-wave technology have led to a resurgence of activity in very-high-frequency (VHF, higher than 150 GHz) electron paramagnetic resonance (EPR) [1]. However, there has been a notable absence of single-crystal studies at VHF, which requires suitable goniometers to perform the crystal rotation. In addition, most VHF research has involved organic systems in amorphous states, for which preparation of suitable single crystals is not easy.

Single-crystal EPR enables a more precise determination of spin-Hamiltonian parameters than is possible from a powder (polycrystalline) system [1, 2]. This is because there are many more data points available from the set of spectra obtained by the rotation of a single crystal with respect to the external magnetic field (B). For each orientation of the single crystal, one has several EPR line positions available to fit to spin-Hamiltonian parameters [2], unlike the case for a powder (polycrystalline) sample for which one only observes broad averages over all orientations at each field value with a concomitant loss of spectral resolution.

Powder linewidths at VHF can be very broad, i.e., in the range of 0.1–1 T in the presence of either large zero-field splittings and/or large *g*-tensor anisotropies [3–5], which seriously reduces the signal-to-noise ratio (S/N) over single-crystal spectra. That is, the resonant susceptibility of a single-crystal sample is enhanced by the cooperative effect of many spins at a given orientation intensifying the transition amplitude of a single line as opposed to a powder sample, where the absorption is averaged over all orientations as noted above, and partitioning of spectral intensity among all transitions reduces the achievable S/N for any one transition. In addition, single crystals have a higher effective spin concentration of the crystalline lattice as opposed to the looser packing of polycrystalline powders. Both effects combined together can lead to a significant improvement of S/N of a single-crystal spectrum as opposed to that for a powder spectrum.

A more precise determination of spin-Hamiltonian parameters can be accomplished by combining low- and high-frequency EPR studies since, in general, the fine-structure zero-field splitting and hyperfine structure parameters A and B are determined more precisely at lower frequencies [6], while the *g*-tensor is determined more precisely at higher frequencies. This is true provided that the zero-field splitting parameter b_2^0 (also denoted as D) is small compared to the Zeeman interaction. Otherwise, the allowed fine-structure transitions may not even be observed at low frequencies. In that case, one has to use an appropriate high frequency. Furthermore, at high enough frequencies where the Zeeman interaction dominates, the EPR spectra are considerably simplified [3, 4].

An additional virtue of single-crystal studies is that the relative intensities of the extreme allowed single-crystal EPR lines observed at low enough temperatures, depending on source frequency, (i.e., $T < h\nu/k$), are compared with those at room temperature for **B** parallel to the magnetic z-axis in the crystal, one can determine the absolute sign of the zero-field splitting parameter D, and thereafter of all other fine-structure parameters, since the least-squares fitting program yields the correct relative signs of all the fine-structure parameters [2].

Although there have been a number of powder VHF EPR studies of transition-metal ions [1, 5], to our knowledge, there have not been reported any orientation-dependent single-crystal EPR studies at VHF [7]*. Allgeier et al. [8], in the context of biological systems, and Haindl et al. [9], in the context of reaction centers in photosynthesis, reported hyperfine single-crystal studies on organic crystals at W-band (95 GHz). These systems with spin $S = 1/2$, have no zero-field splitting parameters, since $S < 1$. Recently, Schwartz et al. [10] and Hill et al. [11] published EPR studies on single-crystal systems with $S > 1/2$. In ref.

---

* In the study reported in ref. 7, the powder of microcrystals aligned in the strong magnetic field, producing an effective single-crystal spectrum with the magnetic z-axis parallel to **B** in a VHF study of Mn^{3+} in Mn(TPP)Cl, Mn(ODMAPz)Cl, Mn(ODMAPz)DTC, and Mn(DD-IX-DME)Cl at frequencies of 200 GHz and higher.

10 studies at 30–120 GHz on neutron-irradiated white sapphire, Al_2O_3, containing Cr^{3+}: $S = 3/2$ and Fe^{3+}: $S = 5/2$, were reported, while in ref. 11 studies at 95 GHz on Mn_{12} cluster complex: $Mn_{12}O_{12}(CH_3COO)_{16}(H_2O)_4$ with $S = 10$, were reported. Resonant cavities were used in both the studies in refs. 10 and 11, unlike the 249.9 GHz measurements reported here, where a Fabry-Pérot resonator was used, as is appropriate for the VHF range.

Our capability for single-crystal rotation at 249.9 GHz, and, equally important, the need to measure large zero-field splittings, which is more difficult at low frequencies, has motivated the study presented in this paper on three transition-metal ions in inorganic crystals.

2 Experimental Arrangement

The 249.9 GHz measurements were carried out at 253 K at Cornell University on a spectrometer that uses a transmission Fabry-Pérot resonator and a superconducting magnet with magnetic field up to 9.4 T, with field modulation in the range of 0.1–0.5 mT at 100 kHz [12–14]. The Q- and X-band measurements were made on Varian and Bruker spectrometers, respectively, at Concordia University; the latter was equipped with an Oxford Instruments helium gas-flow cryostat. The X-band measurements were carried out at room (295 K), liquid nitrogen (77 K), and liquid helium (4.2 K) temperatures and in the temperature range of 120–300 K, while those at Q-band at 295 and 77 K.

The goniometer constructed for single-crystal rotation has been described in [14].

3 Experimental Results and Analysis of Data

3.1 Ni^{2+} *in* $Ni_2CdCl_6 \cdot 2H_2O$

Background. Ni^{2+} is a non-Kramers $S = 1$ ion. Single-crystal X-band EPR studies on $Ni_2CdCl_6 \cdot 12H_2O$, where Ni^{2+} is characterized by a large zero-field splitting, have been reported by Misra et al. [15]. They found two magnetically inequivalent Ni^{2+} ions in the crystal, characterized by the values of the zero-field splitting parameters $D = -31.12$ and -6.81 GHz at 295 K; these values were respectively found to increase and decrease with decreasing temperature. The magnetic *z*-axes of the two inequivalent ions were found to be coincident and parallel to the crystallographic *c*-axis. The two sets of spectra exhibited axial symmetry. At 9.6 GHz, it is still possible to get an observable transition, although the Zeeman interaction is small compared to the zero-field splitting of 31 GHz. (If the zero-field splitting is larger than about 45 GHz, it would not be possible to observe any transition at 9.6 GHz for fields below 1 T.) At 249.9 GHz, the allowed transitions are well in the high-field regime where the Zeeman term dominates. In Fig. 1 energy-level diagrams corresponding to these two sites appropriate for 9.6 and 249.9 GHz resonances, respectively, are shown.

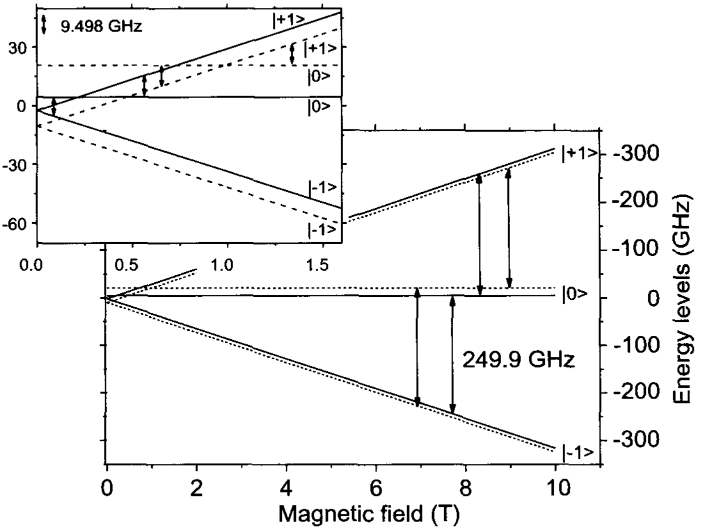

Fig. 1. Plot of the eigenvalues of the Ni^{2+} ion in $Ni_2CdCl_6 \cdot 12H_2O$, calculated with the parameters listed in Table 1, versus the intensity of the external magnetic field B ($\mathbf{B} \parallel z$-axis) showing all expected $\Delta M = \pm 1$ transitions at 249.9 GHz. $D = -6.78$ GHz: solid lines, site I; $D = -30.97$ GHz: dotted lines, site II. The inset shows the eigenvalues versus B ($\mathbf{B} \parallel z$-axis) showing all expected $\Delta M = \pm 1$ transitions at X-band (9.498 GHz). (In order to determine the absolute sign of the zero-field splitting parameter D, one needs to compare the intensities of the extreme lines, $+1 \leftrightarrow 0$ and $0 \leftrightarrow -1$ transitions. As seen in the inset, only one extreme transition is observed at X-band.)

EPR spectra at 249.9 GHz. Measurements were carried out at 253 K for rotations about an axis perpendicular to the crystallographic c-axis, as shown in ref. 14. An inspection of these spectra reveals that there, indeed, exist two magnetically inequivalent Ni^{2+} ions with coincident magnetic axes parallel to the c-axis, and that the previously reported values of D at X-band [15] are correct for both sites. The relative intensities of the broad and narrow components are also consistent with the assignments given in ref. 15. Their respective linewidths of about 100 and 60 mT are comparable to what was observed at 9.6 GHz. The same order of linewidths at 9.6 and 249.9 GHz is most likely due to compensating effects of two competing mechanisms: (i) g-distribution which increases the linewidth with increasing frequency; and (ii) exchange narrowing, (i.e., the 10/3 effect) which decreases the linewidth with increasing frequency (see ref. 16, and references therein). The 249.9 GHz spectra show only a small deviation from an isotropic g-value, but it is within the error bounds consistent with the previous report [15]. Since the Zeeman interaction dominates the zero-field splitting, these spectra are very easy to interpret. In fact, the magnitudes of the zero-field splitting are easily read from the high-frequency spectra unlike the case for X-band.

Spin-Hamiltonian parameters. The spin-Hamiltonian, assuming that the principal axes of the g and zero-field splitting tensors are coincident, describing this system is:

$$\mathscr{H} = \mu_B[g_\parallel B_z S_z + g_\perp(B_x S_x + B_y S_y)] + D[S_z^2 - S(S+1)/3] + E(S_x^2 - S_y^2). \qquad (1)$$

In Eq. (1), μ_B is the Bohr magneton, and the subscripts x, y, z represent the components along the magnetic axes, for which orientations of **B** the splitting of allowed lines exhibit extrema [15]. The spin-Hamiltonian parameters were evaluated with a least-squares procedure in conjunction with matrix diagonalization [2], fitting simultaneously all resolved EPR line positions observed at 9.49 GHz (295 K) and at 249.9 GHz (253 K), assuming that the temperature variation of spin-Hamiltonian parameters between these two temperatures is not significant (Table 1). These combined results are in good agreement with those previously obtained from 9 GHz; i.e., we may regard the 249.9 GHz spectra as confirming the zero-field splitting parameters. In addition, we obtained more accurate g-tensor parameters, i.e., an additional significant figure compared to lower-frequency fits, solely from the 249.9 GHz spectra. As noted previously, this is because the g-tensor effects are more important in the high-field spectra.

3.2 Mn^{2+} in ZnV_2O_7

Background. Pyrovanadate oxides of Zn, undergoing a phase transformation at 615°C with reducing oxygen coordination of the cation, have been investigated by X-ray diffraction [17] and by phase-diagram studies of the ZnO-V_2O_5 system [18]. EPR studies of the Mn^{2+} ion in single crystals, similar in structure to the thortveitite structure of high-temperature β-phase $Zn_2V_2O_7$, have been reported. Stager [19] investigated EPR of Mn^{2+} in $Cd_2V_2O_7$, while Chambers et al. [20] recorded Mn^{2+} and Cu^{2+} EPR spectra, studying the structural phase transition in single crystals of $Zn_2P_2O_7$ from high-temperature thortveitite structure to a low-symmetry phase occurring at lower temperature. V^{4+} EPR spectra in conjunction with electrical conductivity were investigated by Ioffe et al. [21] in single crystals of low-temperature α-phase $Zn_2V_2O_7$. Mn^{2+} EPR studies have not so far been reported in this crystal, possibly because of the complexity of the EPR spectrum

Table 1. Spin-Hamiltonian parameters for Ni^{2+} in $Ni_2CdCl_6 \cdot 12H_2O$ single crystal. Here SMD(GHz^2) = $\sum_i(\Delta E_i^{\mathrm{cal}}/h - \nu_i)^2/\sigma_i^2$; σ_i = 1 and 10 for each data point at 9.49 and 249.9 GHz, respectively. ΔE_i is the calculated energy difference between the levels participating in resonance for the ith line position, ν_i being the corresponding klystron frequency, and h is the Planck constant. RMSL (GHz) ≡ (SMD/n)$^{1/2}$ represents the mean deviation per fitted line position from the microwave frequency, where n is the number of fine-structure line positions fitted simultaneously. The g-tensor values obtained just from 249.9 GHz data are also included.

Site	ν (GHz)/T (K)	$g_\parallel$	$g_\perp$	b_2^0 (GHz)	RMSL
Site I	9.49/295 and 249.9/253	2.245±0.024	2.257±0.028	−6.781±0.140	0.25
	249.9/253	2.230±0.003	2.226±0.003		
Site II	9.49/295 and 249.9/253	2.244±0.026	2.207±0.007	−30.97±0.449	0.37
	249.9/253	2.226±0.003	2.219±0.003		

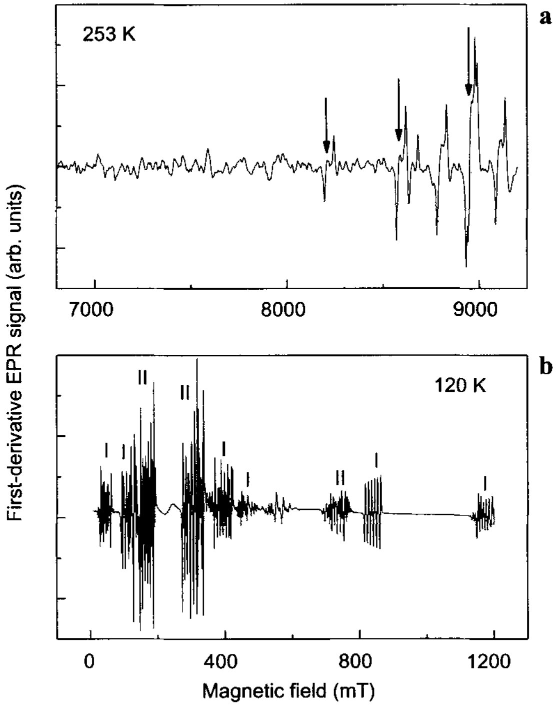

Fig. 2. 249.9 GHz (**a**) and 9.615 GHz (**b**) EPR spectra of the Mn^{2+} ion in the $Zn_2V_2O_7$ single crystal for the orientation of the magnetic field **B** along the magnetic *Z*-axis of one inequivalent ion, which is coincident with the magnetic *X*-axis of the other inequivalent ion. In **b**, the lines for the former Mn^{2+} ion are marked as I, while those for the other Mn^{2+} ion as II. In **a**, the vertical arrows indicate the transitions corresponding to the former ion.

and a rather large value of the Mn^{2+} zero-field splitting parameter ($b_2^0 \approx 6$ GHz, as determined here).

EPR spectra. EPR spectra for the Mn^{2+} ion were recorded in a single crystal of α-$Zn_2V_2O_7$ at X-band (9.6 GHz) and far-infrared (FIR) (249.9 GHz) frequencies. There were found two magnetically inequivalent, but physically equivalent, Mn^{2+} ions as determined here from the EPR spectra. Figure 2 shows the Mn^{2+} EPR spectra at 9.6 GHz (120 K) and 249.9 GHz (253 K), for the orientation of the external magnetic field at **B** parallel to (Z_1, Y_1), magnetic axes of the two magnetically inequivalent Mn^{2+} ions 1 and 2. The ^{55}Mn nucleus (100% natural abundance) has the nuclear spin $I = 5/2$ ($g_n = 1.382$); thus, each fine-structure line splits into six hyperfine lines at X-band. Resolution of hyperfine lines was not fully observed at 249.9 GHz (see Sect. 4). From the EPR spectra, the magnetic *Y*-axes of the two magnetically inequivalent Mn^{2+} ions were found to be coincident. The *Z*-axes of these two ions were found to be in the perpendicular plane at about 90° from each other. Thus, the *Z*-axis of one ion and the *X*-axis of the other ion are almost coincident. Both sets of EPR lines were found

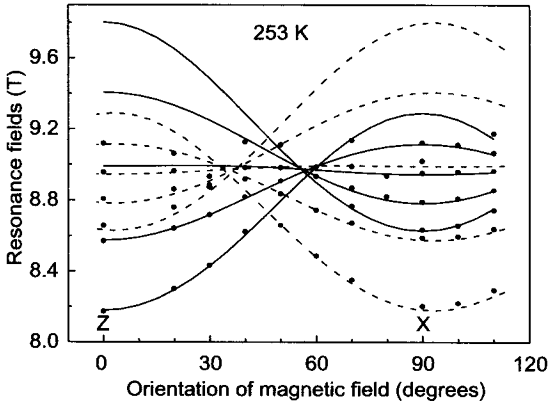

Fig. 3. Angular variation of Mn^{2+} EPR lines at 249.9 GHz in the $Zn_2V_2O_7$ single crystal in the *ZX*-plane. The fine-structure lines belonging to the two magnetically inequivalent Mn^{2+} ions are shown. The points represent experimental data, while the solid and dotted lines represent the calculated line positions for the two inequivalent ions with the spin-Hamiltonian parameters listed in Table 2.

to be described by the same set of spin-Hamiltonian parameters, the two magnetically inequivalent ions being physically equivalent.

Spin-Hamiltonian parameters. The EPR line positions were fitted to a spin Hamiltonian appropriate to monoclinic site symmetry, expressed as follows [22]:

$$\mathscr{H} = \mu_B g(B_zS_z + B_xS_x + B_yS_y) + \sum_{n=2,4}^{m=0,\pm2,\pm4} \alpha_n b_n^m O_n^m + AS_zI_z + B(S_xI_x + S_yI_y)\,. \quad (2)$$

In Eq. (2), $S = 5/2$ and $I = 5/2$ are the electronic and nuclear spins of the Mn^{2+} ion, respectively; an isotropic *g*-tensor was used taking into account the S-state of the Mn^{2+} ion; the b_n^m are the spin-Hamiltonian parameters with $\alpha_n = 1/3$ and 1/60 for $n = 2$ and 4, respectively; the O_n^m are the Stevens spin operators [16, 23]; the *A* and *B* are hyperfine-interaction constants; and the quadrupolar-interaction terms are neglected.

The angular variations of the Mn^{2+} fine-structure line positions as observed and calculated at 249.9 GHz (253 K) for the two magnetically inequivalent Mn^{2+} ions are displayed in Fig. 3.

Since this is a case of an isotropic *g*-tensor, VHF EPR only offers some improvement in the accuracy of the average *g*-value (see Table 2). The angular variations of the line positions at 249.9 GHz shown in Fig. 3 are simpler than those at 9.6 GHz due to the fact that the former, being in the high-field limit, yield a simple fine-structure pattern from which a very good first approximation to the b_2^0 can be read directly from the spectrum, (see refs. 3 and 4 for a discussion of this in powder samples of Mn^{2+}). The combined 249.9 and 9.6 GHz results for b_2^0 and b_2^2 agree within experimental error with those determined just from 9.6 GHz data at 295 K, but there are significant differences in the values

Table 2. Spin-Hamiltonian parameters for Mn^{2+} in $Zn_2V_2O_7$ single crystal. The fitted parameter α is the misorientation angle in the *ZX* plane and is different at different frequencies due to the crystal being placed separately within the respective resonators. RMSL represents the mean deviation per fitted line position from the microwave frequency. The magnetic axes X_i, Y_i, Z_i; $i = 1, 2$ for the two magnetically inequivalent ions are such that $Y_1 \parallel Y_2$, $Z_1 \parallel X_2$, $X_1 \parallel Z_2$. The Y_1 ,Y_2 axes lie in the cleavage, (110), plane of the crystal, while the X_1 ($\parallel Z_2$), Z_1 ($\parallel X_2$) axes lie in the plane perpendicular to the cleavage plane as well as being parallel to the $Y_1 \parallel Y_2$ axes, at ±45° with the cleavage plane. *n* and RMSL are defined in Table 1.

	ν (GHz)/*T* (K)				
Parameter	9.61/295 (249.9/253)	9.61/295	9.61/120	9.61/77	9.61/4.2
g	2.000±0.003	2.008±0.006	2.007±0.006	2.007±0.006	2.09±0.09
α (°)	1.27 (−0.05)	1.27±0.03	0.44±0.03	0.38±0.03	−3.9±0.03
b_0^2 (GHz)	5.72±0.02	5.75±0.02	6.05±0.02	6.08±0.02	6.15±0.50
b_2^2 (GHz)	1.08±0.02	1.09±0.02	1.08±0.02	1.03±0.02	1.11±0.50
b_4^0 (GHz)	−0.05±0.01	−0.23±0.01	−0.20±0.01	−0.09±0.01	0.11±0.05
b_4^2 (GHz)	−0.59±0.01	−0.73±0.01	−0.18±0.01	0.05±0.01	1.17±0.05
b_4^4 (GHz)	−0.25±0.01	−0.15±0.01	−0.50±0.01	−0.40±0.01	−0.28±0.05
A (GHz)		−0.236±0.001	−0.236±0.001	−0.236±0.001	−0.236±0.001
B (GHz)		−0.236±0.001	−0.236±0.001	−0.236±0.001	−0.236±0.001
n	101	60	55	40	71
RMSL (GHz)	0.18	0.22	0.21	0.11	0.29

of the smaller parameters b_4^m. Further studies are needed to determine what significance to attach to this (see Sect. 4).

3.3 Fe^{3+} in $YCaAlO_4$

Background. $YCaAlO_4$ is an interesting crystal because its structure is similar to the superconducting oxide materials, such as $La_{2-x}Sr_xCuO_4$, and this material can be used as a solid-state laser [24] owing to the large crystal field splitting, resulting in a very large zero-field splitting parameter, b_2^0, in this crystal. EPR on the ions Ti^{3+}, V^{4+}, and Cr^{3+} was investigated in $YCaAlO_4$ by Yamaga et al. [25–27]. It is thus ideal for VHF EPR studies.

EPR spectra. Fe^{3+} EPR spectra were recorded on an $YCaAlO_4$ single crystal at X-band (4.2–295 K), Q-band (77, 295 K), and FIR (253 K) frequencies. They are shown in Fig. 4 for the orientation of the external magnetic field along the magnetic *Z*-axis at X- and Q-band, while at 10° from the magnetic *Z*-axis at 249.9 GHz. The spectra reveal the existence of two magnetically inequivalent Fe^{3+} ions, as seen from Fig. 4a for X-band, with roughly equal concentrations of each as estimated from integrated intensities. One magnetically inequivalent ion has its *Z*-axis along the *c*-axis of the crystal and linewidths of about 10 mT, while the other magnetically inequivalent ion has its *Z*-axis at about 50° from the *Z*-axis of the former. The former ion enters the lattice substitutionally as revealed by the orientation of its *Z*-axis, and we focus in this paper only on this ion.

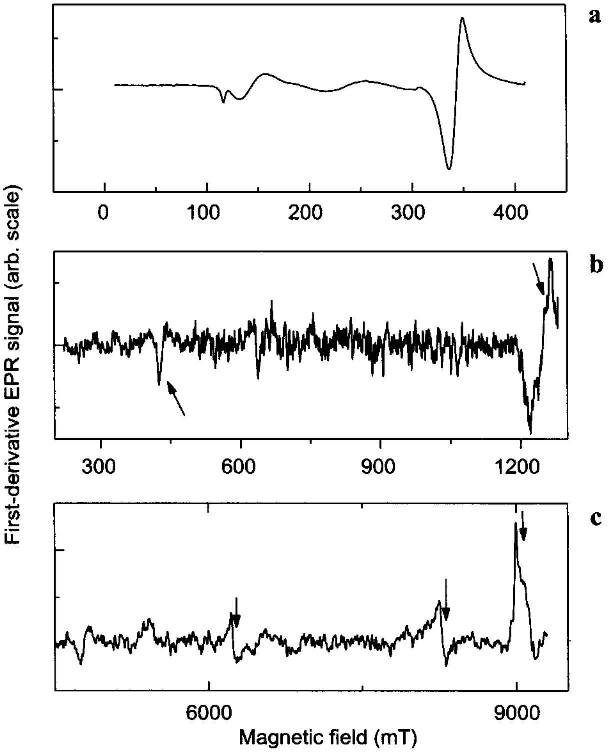

Fig. 4. EPR spectrum of the Fe^{3+} ion in $YCaAlO_4$ at: **a** 9.79 GHz and 295 K for **B** along the magnetic Z-axis; **b** 35.69 GHz and 295 K for **B** along the magnetic Z-axis; **c** 249.9 GHz and 253 K for **B** at 10° from the magnetic Z-axis in the ZX-plane.

Spin-Hamiltonian parameters. The following spin Hamiltonian appropriate to tetragonal symmetry, with the same definitions as those used in Eq. (2), and $m \leq n$, was used to fit the EPR line positions to evaluate the spin-Hamiltonian parameters:

$$\mathcal{H} = \mu_B(g_\parallel B_z S_z + g_\perp(B_x S_x + B_y S_y) + \sum_{n=2,4}^{m=0,4} \alpha_n b_n^m O_n^m . \tag{3}$$

Here again $S = 5/2$; $\alpha_n = 1/3$ and 1/60, respectively, for $n = 2$ and 4, but unlike Eq. (2) there are no hyperfine terms. This is again a case where, in high field (e.g., 9 T) the spectrum is expected to be a simple one consisting of the five $\Delta M = \pm 1$ transitions separated by the zero-field splitting.

There are two main problems in the determination of the spin-Hamiltonian parameters from X-band EPR line positions in this crystal. First, the EPR lines are almost completely broadened out for magnetic field values higher than 0.35 T at X-band. Unfortunately, the positions of these high-field EPR lines depend on b_2^0, and they would have been useful to estimate this parameter were they available for the fitting. Second, in this crystal, due to the large Fe^{3+} zero-field splitting ($D \sim 29$ GHz), there result three well-separated Kramers doublets $M = \pm 5/2$, $M = \pm 3/2$, and $M = \pm 1/2$ at X-band, within which the EPR transitions occur. The observation of forbidden EPR transitions is possible within the first two doublets due to the mixing of levels by the spin-Hamiltonian term $b_4^4 O_4^4$. Since full angular variation was observed only for the $+1/2 \leftrightarrow -1/2$ transition, only the EPR line positions for this transition for the orientation of **B** near the $X(Y)$ magnetic axis can be used to estimate b_2^0. This is because for **B** near the Z-axis, the dependence of this line on b_2^0 manifests itself only in the second order in perturbation theory, whereas for **B** near the $X(Y)$-axis this dependence is in the first order, due to the transformation of the spin operators [23]. Thus, it would be helpful to fit EPR line positions corresponding to allowed fine-structure transitions other than $+1/2 \leftrightarrow -1/2$ observed at 249.9 GHz to estimate the zero-field splitting parameter D precisely, since these transitions depend on D in zero-order of perturbation. Unfortunately, only four such transitions were observed with the Schottky diode detector (see Sect. 4).

The spin-Hamiltonian parameters for the Fe^{3+} ion in the single crystal of $YCaAlO_4$ were determined from a simultaneous fitting of EPR line positions obtained at several orientation of the external magnetic field with respect to the crystal axis with the least-squares-fitting/matrix-diagonalization procedure [2] at 9.79 and 35.67 ($T = 295$ K), and 249.9 GHz ($T = 253$ K). The resulting values are $g_{\parallel} = 1.992 \pm 0.015$, $g_{\perp} = 1.987 \pm 0.015$, $b_2^0 = 29.341 \pm 0.720$ GHz, $b_4^0 = -3.975 \pm 0.483$ GHz, $b_4^4 = 4.112 \pm 0.497$ GHz, RMSL = 0.27 GHz ($\sigma_i = 1$, 3 and 10). The magnetic z-axes for the two magnetically inequivalent ions have the following orientation parallel and at 52° from the crystallographic c-axis for ions I and II, respectively. Since no information on the morphology of the crystal relating the crystal faces to the crystallographic planes is available, it was not possible to relate all the magnetic axes to the crystallographic axes. However, taking into account the similarity of the crystallographic axes for the Cr^{3+} ion in the same crystal as determined by Yamaga et al. [27–29], the x, y magnetic axes for the ion I could be along the [110], $[1\bar{1}0]$ directions, respectively. For the ion II the orientation of the x, y magnetic axes is difficult to determine from our data.

4 Discussion

On the basis of the results of Sect. 3, we discuss virtues and limitations of single-crystal EPR studies at VHF, as well as aspects that lead to further improvement.

Some advantages of single-crystal studies over the use of powders are S/N and resolution. This comparison can most conveniently be done by simulating the powder spectra expected for the spin-Hamiltonian parameters given in Sect. 3, and then comparing them with the single-crystal results (both experimental and simulations), rather than crushing and powdering the single crystals. When this is done, we find, as expected, that the powder spectra are generally much broader, thereby reducing both signal sensitivity and spectral resolution. For example, for the case of Mn^{2+} in ZnV_2O_7, where all 5 fine-structure lines are prominent and of comparable amplitude in the single-crystal spectra, only the central line ($+1/2 \leftrightarrow -1/2$) is not severely broadened in the powder. (We recall that in our experiments we just observe the 3 lines occurring below 9.4 T.) The others are only a few percent of the amplitude of the central line, which itself is less intense by about a factor of 3 than the single-crystal line.

We now address some virtues of VHF single-crystal EPR illustrated or suggested by these studies.

Determination of large zero-field splittings. The examples of Mn^{2+} and Fe^{3+} show that an important advantage is the ability to measure very large zero-field splitting ($D > 20$ GHz), which is typical in biological systems, such as metalloproteins [28]. At low microwave frequencies, with the typical available magnetic fields, e.g., lower than 1 T at X-band and lower than 2.5 T at Q-band, one can at most address a subset of $\Delta M = \pm 1$ transitions other than $1/2 \leftrightarrow -1/2$, necessary to estimate D, if there are any at all depending on the value of the zero-field splitting parameter D.

For the Kramers case, this can be seen in Fig. 5, which shows the energy level scheme as well as the $\Delta M = \pm 1$ transitions that can be observed at 9.79, 35.69, and 249.9 GHz for Fe^{3+} in $YCaAlO_4$ with the parameters determined at 295 and 253 K as listed in Sect. 3.3. (Some of the same $\Delta M = \pm 1$ transitions can be observed at more than one magnetic field position.) At 249.9 GHz it is possible to observe all $\Delta M = \pm 1$ transitions, provided the external magnetic field can be varied up to about 13 T. This is not possible at 9.79 and 35.69 GHz, as seen from Fig. 5, where $\Delta M = \pm 1$ transitions exist below 5 T that are not attainable at these frequencies. The ability to observe all $\Delta M = \pm 1$ transitions is important to estimate the values of the zero-field splitting parameters accurately. In addition, when one tries to determine the absolute sign of D, and thus those of all the spin-Hamiltonian parameters since the least-squares fitting/matrix-diagonalization procedure yields correct relative signs of all the parameters [2], this requires comparing the intensities of the two extreme lines belonging to the whole set of $\Delta M = \pm 1$ transitions [16].

The case for non-Kramers ions is suggested by Fig. 1, showing the energy levels for Ni^{2+}. One can observe $\Delta M = \pm 1$ transitions at X-band for values of D up to about 40 GHz, from which D may be extracted from a rotational set of spectra. On the other hand, when D is significantly larger than 40 GHz, HF-EPR becomes essential, as was the case for another non-Kramers ion Mn^{3+} with $S = 2$ investigated by Goldberg et al. [7] ($D \sim 66$ GHz).

More accurate determination of g-tensor. In general, our results are consistent with more accurate g-tensors (for Ni^{2+}) or g-factor for isotropic cases (Mn^{2+} and Fe^{3+}) obtainable at VHF.

Improvements of S/N and spectral resolution. Very recently, we have found that by replacing the Schottky detector with an In-Sb bolometer [13, 14] we could improve S/N by a factor of 5–10. Improvements in the mechanical and thermal

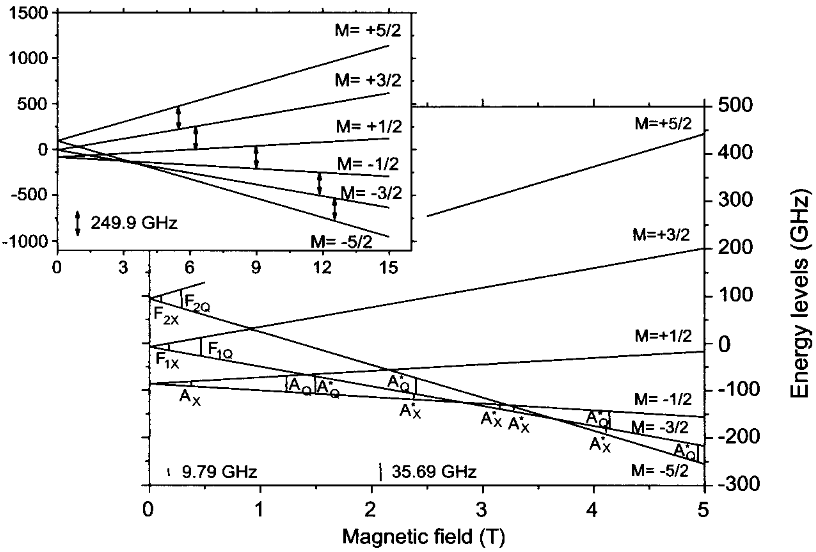

Fig. 5. Plot of the eigenvalues of the Kramers Fe^{3+} ion in $YCaAlO_4$, calculated with the parameters listed in Sect. 3.3, versus the intensity of the external magnetic field B ($\mathbf{B} \parallel z$-axis) showing all expected $\Delta M = \pm 1$ transitions at X- (9.79 GHz) and Q- (35.69 GHz) bands. A_X and A_Q, allowed transitions, $\Delta M = \pm 1$; F_{1X} and F_{1Q}, forbidden transitions, $\Delta M = \pm 3$; F_{2X} and F_{2Q}, forbidden transitions, $\Delta M = \pm 5$; subscript X refers to X-band, subscript Q refers to Q-band, $D = 29.34$ GHz, $g_x = g_z = 1.99$. The inset shows the eigenvalue plot versus B ($\mathbf{B} \parallel z$-axis) showing all expected $\Delta M = \pm 1$ transitions at 249.9 GHz.

stability of the FP resonator used in this work allowed for a further improvement in S/N by a further factor of about 2. In addition we found that despite the wide sweep ranges of several Tesla required, it is important to use very slow sweep rates. For example, with sweep rates of 0.5 mT/s instead of the rate of 2.5 mT/s used in the above studies, it was possible to obtain extremely narrow lines for Mn^{2+} in ZnV_2O_7, which showed well-resolved hyperfine structure at 249.9 GHz, comparable to those observed at 9.6 GHz. This is consistent with previous work performed in this laboratory on S-state ions [29]. The analysis of these much more complex spectra is currently in progress. Finally we note that by working at low temperatures (ca. 10 K) additional improvement in S/N can be achieved.

Acknowledgements

S.K.M. and S.I.A. are grateful to the Natural Sciences and Engineering Research Council of Canada for partial financial support. This work was supported by grants from the NIH/NCRR and NSF. Computations were facilitated by the resources of the Cornell Theory Center.

References

1. Freed J.H.: Annu. Rev. Chem. **51**, 655 (2000)
2. Misra S.K.: J. Magn. Reson. **23**, 406 (1976)
3. Lynch W.B., Boorse R.S., Freed J.H.: J. Am. Chem. Soc. **115**, 10909 (1993)
4. Wood R.M., Stucker D.M., Jones L.M., Lynch W.B., Misra S.K., Freed J.H.: Inorg. Chem. **38**, 5384 (1999)
5. Hagen W.R.: Coord. Chem. Rev. **190–192**, 209 (1999)
6. Misra S.K.: Physica B **240**, 183 (1997)
7. Goldberg D.P., Tesler J., Krzystek J., Montalban A.G., Brunel L.-C., Barrett A.G.H., Hoffman B.M.: J. Am. Chem. Soc. **119**, 8722 (1997)
8. Allgeier J., Disselhorst J.J.J.M., Weber R.T., Wenkenbach W.Th., Schmidt J. in: Modern Pulse and Continuous Wave ESR (Kevan L., Bowman M.K., eds.), chap. 6. New York: Wiley 1990.
9. Haindl E., Möbius K., Oloff H.: Z. Naturforsch. A **40**, 169 (1985)
10. Schwartz D.A., Walter E.D., McIlwain S.J., Krymov V.N., Singel D.J.: Appl. Magn. Reson. **16**, 223 (1999)
11. Hill S., Dalal N.S., Brooks J.S.: Appl. Magn. Reson. **16**, 237 (1999)
12. Lynch W.B., Earle K.A., Freed J.H.: Rev. Sci. Instrum. **59**, 1345 (1988)
13. Earle K.A., Budil D.E., Freed J.H. in: Advances in Magnetic and Optical Resonance (Warren W.S., ed.), vol. 19, pp. 253–323. New York: Academic Press 1996.
14. Earle K.A., Freed J.H.: Appl. Magn. Reson. **16**, 247 (1999)
15. Misra S.K., Misiak L.E., Chand P.: Physica B **202**, 31 (1994)
16. Abragam A., Bleaney B.: Electron Paramagnetic Resonance of Transition Ions. Oxford: Clarendon Press 1970.
17. Gopal R., Calvo C.: Can. J. Chem. **51**, 1004 (1973)
18. Brown J.J., Hummel F.A.: Trans. Br. Ceram. Soc. **64**, 419 (1965)
19. Stager C.V.: Can. J. Phys. **46**, 807 (1968)
20. Chambers J.G., Datars W.R., Calvo C.: J. Chem. Phys. **41**, 806 (1964)
21. Ioffe V.A., Grunin V.S., Zonn Z.N., Ivanov S.E., Yanchevskaya I.S.: Izv. Akad Nauk SSSR, Neorg. Mater. **13**, 1843 (1977)
22. Misra S.K., Rudowicz C.Z.: Physica B **147**, 677 (1988)
23. Misra S.K. in: Handbook of Electron Spin Resonance (Poole C.P., Farach H.A. Jr., eds.), chap. VII, p. 115. New York: A.I.P. Press, Springer 1999.
24. Yamaga M., Macfarlane P.I., Holliday K., Henderson B., Kodama N., Inoue Y.: J. Phys. Condens. Matter **8**, 3487 (1996)
25. Yamaga M., Yosida T., Naitoh Y., Kodama N.: J. Phys. Condens. Matter **6**, 4381 (1994)
26. Yamaga M., Henderson B., Yosida T., Kodama N., Inoue Y.: Phys. Rev. B **51**, 3438 (1995)
27. Yamaga M., Yosida T., Fukui M., Takeuchi H., Kodama N., Inoue Y., Henderson B., Holliday K., Macfarlan P.I.: J. Phys. Condens. Matter **8**, 10633 (1996)
28. Misra S.K in: Instrumental Methods in Electron Magnetic Resonance (Bender C., Berliner L., eds.), vol. 18. Dordrecht: Kluwer Academic/Plenum Publications 2002, in press.
29. Clarkson R.B., Smirnov A.I., Smirnova T.I., Kang H., Belford R.L., Earle K.A., Freed J.H.: Mol. Phys. **95**, 1325 (1998)

Authors' address: Jack H. Freed, Baker Laboratory, Department of Chemistry and Chemical Biology, Cornell University, Ithaca, New York 14853-1301, USA